NeuroImage 52 (2010) 1268–1278

Contents lists available at ScienceDirect

NeuroImage

journal homepage: www.elsevier.com/locate/ynimg

Transcranial direct current stimulation in patients with skull defects and skull plates: High-resolution computational FEM study of factors altering cortical current flow

Abhishek Datta [a,*], Marom Bikson [a], Felipe Fregni [b,c,*]

[a] Neural Engineering Laboratory, Department of Biomedical Engineering, The City College of New York of CUNY, New York, NY 10031, USA
[b] Laboratory of Neuromodulation, Spaulding Rehabilitation Hospital, Harvard Medical School, Boston, MA 02114, USA
[c] Berenson-Allen Center for Noninvasive Brain Stimulation, Beth Israel Deaconess Medical Center, Harvard Medical School, Boston, MA, 02215, USA

ARTICLE INFO

Article history:
Received 3 November 2009
Revised 13 March 2010
Accepted 24 April 2010
Available online 7 May 2010

Keywords:
tDCS
TBI
Skull defects
Skull plates
Finite element modeling
MRI human head model

ABSTRACT

Preliminary positive results of transcranial direct current stimulation (tDCS) in enhancing the effects of cognitive and motor training indicate that this technique might also be beneficial in traumatic brain injury or patients who had decompressive craniectomy for trauma and cerebrovascular disease. One perceived hurdle is the presence of skull defects or skull plates in these patients that would hypothetically alter the intensity and location of current flow through the brain. We aimed to model tDCS using a magnetic resonance imaging (MRI)-derived finite element head model with several conceptualized skull injuries. Cortical electric field (current density) peak intensities and distributions were compared with the healthy (skull intact) case. The factors of electrode position (C3-supraorbital or O1-supraorbital), electrode size skull defect size, skull defect state (acute and chronic) or skull plate (titanium and acrylic) were analyzed. If and how electric current through the brain was modulated by defects was found to depend on a specific combination of factors. For example, the condition that led to largest increase in peak cortical electric field was when one electrode was placed directly over a moderate sized skull defect. In contrast, small defects midway between electrodes did not significantly change cortical currents. As the conductivity of large skull defects/plates was increased (chronic to acute to titanium), current was shunted away from directly underlying cortex and concentrated in cortex underlying the defect perimeter. The predictions of this study are the first step to assess safety of transcranial electrical therapy in subjects with skull injuries and skull plates.

Introduction

Transcranial electrical stimulation using weak direct currents – transcranial direct current stimulation (tDCS) – is a promising method of brain modulation that has been increasingly tested as a tool to modulate plasticity in neuropsychiatric diseases (Boggio et al., 2009b). Relatively simple to apply, tDCS involves application of direct current through at least one electrode positioned on the scalp. The mechanisms of tDCS are associated with the intensity and direction of current flow through the cortex, leading to neuromodulation and lasting changes in cortical excitability. The polarity specific shifts in cortical excitability have been suggested to be due to membrane polarization (Ardolino et al., 2005; Radman et al., 2009) leading to modulation of sodium and calcium channel conductance and a change in NMDA-receptor activation (Liebetanz et al., 2002; Nitsche et al., 2003). Clinical tDCS has shown to induce beneficial effects in preliminary studies in different neuropsychiatric conditions such as pain (Fregni et al., 2006a; 2007), motor rehabilitation (Fregni et al., 2005b; Hummel et al., 2005), cognitive function (Fregni et al., 2005a; Iyer et al., 2005), major depression (Boggio et al., 2007) and craving disorders (Boggio et al., 2009a).

Because of these initial positive results, tDCS has the potential to be used for the rehabilitation of patients with brain lesions who also have skull defect (with or without skull plates) such as patients with traumatic brain injury (TBI) or patients who undergo neurosurgery. In fact, some of the neurological sequelae are presumably consequences of disrupted cortical activity following the traumatic event, and tDCS in this circumstance can be a useful tool to reactivate and restore activity in essential neural networks associated with cognitive and motor processing. In our pilot study combining tDCS with robotic motor training aimed at upper extremity motor recovery, in a small group of TBI survivors with no skull defects, we showed that tDCS can enhance the effects of upper extremity motor training (Chew et al., 2009). tDCS has similar potential to also improve cognition in these patients. Finally, because of preliminary data showing that tDCS reduces epileptogenic activity as indexed by epileptiform discharges in humans and seizure threshold in animals (Fregni et al., 2006b;

* Corresponding authors. A. Datta is to be contacted at T-463 Steinman Hall, Grove School of Engineering, The City College of CUNY, 160 Convent Ave, New York, NY 10031, USA. Fax: +1 212 650 6727. F. Fregni, Spaulding Rehabilitation Hospital, 125 Nashua Street, Boston, MA 02114, USA. Fax: +1 617 975 5322.
E-mail addresses: abhishek.datta@gmail.com (A. Datta), ffregni@partners.org (F. Fregni).

1053-8119/$ – see front matter © 2010 Elsevier Inc. All rights reserved.
doi:10.1016/j.neuroimage.2010.04.252

Liebetanz et al., 2006), this technique might be useful for patients with refractory epilepsy who underwent surgery and have skull plates or applied to patients who needed to undergo decompressive craniectomy for trauma and cerebrovascular disease.

Although evidence supports the investigation of tDCS in TBI or patients with other major neurological deficits and skull defects, one perceived limitation for the use of tDCS in these patients is the modified current flow by the skull defects and use of skull plates. During tDCS, the current applied at the scalp must pass through the resistive skull before reaching the brain, and the specific relationship between electrode position, skull geometry, and the underlying tissue properties are thought to determine the location and magnitude of current flow (Datta et al., 2009a). It remains unknown how skull defects and use of skull plates associated with TBI would affect current flow through the brain and how to modify tDCS dose and/or electrode locations in such cases. For example, a hole through the skull that is filled with relatively highly conductive fluid or tissue, might present an attractive "shunt" pathway for current entering the brain. The underlying cortex would then be exposed to a higher intensity of focused current flow. This in turn might be either beneficial in targeting the underlining brain region or hazardous if the increased current levels resulted in undesired neurophysiologic or pathological changes.

Computational finite element method (FEM) models of tDCS allow prediction of current flow through the cortex (Miranda et al., 2006; Wagner et al., 2007). We previously developed a high-resolution MRI-derived model of tDCS with increased precision and accuracy (Datta et al., 2009a). Here we modify this model to include conceptualized (cylindrical) skull defects and plates and analyze resulting changes in cortical current flow; therefore our aims were to: (i) determine cortical current density distributions in subjects with skull defects; (ii) determine whether the size of skull defect influences the amount and location of current induced in the brain and (iii) determine whether skull plates (i.e. acrylic or titanium plates) also change (and in which direction) the amount of current being delivered to the brain. Our predictions provide a general framework to determine what factors modulate current flow to the brain in cases of specific skull injuries, and thus a rational basis for customizing electrical stimulation dose based on individual parameters and desired outcome.

Methods

Models

To consider the role of skull defects on brain current flow during tDCS, we developed finite element (FE) models that addressed the role of electrode configuration and skull defect size/properties. All models were based on a single MRI-derived head model from a healthy adult subject, where idealized (cylindrical) skull defects were added. For Part 1, we considered two electrode configurations (C3-supraorbital or O1-supraorbital), two defect sizes (2.5 cm and 10 cm diameter), two defect locations in relation to the electrodes (under and between the stimulation pads), and four defect states (acute tissue, chronic tissue, titanium skull plate, and acrylic skull plate). In Part 2, we considered only the effect of incrementally changing the defect size. In each case, the electric fields induced on the cortical surface were compared to the healthy (no defect) case.

MRI guided finite element head model

The volume conductor 3D model (having 1 mm^3 resolution) used in this study was developed previously by our group to calculate tDCS induced electric fields. The entire process involving segmentation of high-resolution 3 T MRI scans, mesh creation and the eventual export to a finite element method solver (SIMPLEWARE LTD., UK) was detailed previously (Datta et al., 2009a); importantly the entire workflow preserves the high resolution of the MRI scans. The model is referred to as the 'healthy head model' in this paper (Fig. 1) and the electrical properties of the tissues are assigned representative isotropic average values (in S/m): brain: 0.2; CSF: 1.65; skull: 0.01; and scalp: 0.465. The muscle, fatty tissue, eyes and blood vessel compartments were assigned the same tissue properties as that of scalp. In this study, the tDCS induced cortical currents of a healthy head was used as a control to evaluate the effects of skull injury. In Part 1, we modeled two electrode *configurations* in combination with a range of skull *defects* and skull *plates*, as specified below. For each model, the combination of electrode configuration and skull injury type and location, together determine the model *montage*. For Part 2, we focused on the role of varying skull defect size under an electrode. Outside of the injury, head properties were unchanged across montages.

Part 1: electrode properties and configurations

We modeled conventional "sponge-based" electrodes having an area of 35 cm^2 (7×5 cm) which is a size commonly used in clinical studies (Fregni et al., 2005a, 2006a) and calculated the induced currents in the cortex resulting from application of 1 mA total current (corresponding to an average electrode surface current density of 0.28 A/m^2).

We modeled two electrode configurations (Fig. 1):

(A) M1-supraorbital: The anode electrode was placed over the primary motor cortex with its center localized 5 cm lateral from the vertex (corresponding to C3) and the cathode electrode was placed over the contralateral supraorbital area.
(B) Occipital-supraorbital: The anode electrode was placed on O1 (primary occipital cortex) and the cathode electrode was placed over the contralateral supraorbital area.

The latter electrode configuration allowed us to model the presence of large skull defects and skull plates between the stimulation electrodes. During conventional tDCS, rectangular sponges are typically soaked in saline and the abutting electrode is energized. The sponge was thus assigned the electrical conductivity of saline ($\sigma = 1.4$ S/m) and the stimulation electrodes were modeled as conductors ($\sigma = 5.8\times10^7$ S/m). The electrodes had a thickness of 1 mm and the thickness of the sponge varied from 1 to 2.5 mm (Datta et al., 2009a). An important note here is that electrode *location* is important in relation to skull defects and skull plates.

Part 1: skull defects — acute and chronic defects

Skull defects were modeled as idealized cylindrical "holes" in the skull. We considered the following two defect sizes in this study: (1) a large hole having a diameter of 10 cm that can be associated with decompression craniectomy, in cases of surgery for hemorrhage drainage in which the removed skull is not placed back, or large skull fracture (Rish et al., 1979) and (2) a small hole with a diameter of 2.5 cm that is usually found as a consequence of a neurosurgical procedure or a small skull fracture (Sekhar and Fessler, 2006). Distinct locations of the holes — either under or between the stimulation electrodes were modeled. In cases where the hole in the skull was underneath the stimulation electrode, the center of the injury was aligned with the center of the electrode (for instance, over the primary motor cortex, corresponding to the location of C3). In cases where the holes were between the stimulation electrodes, the center of the injury corresponded to approximately midway between the anode and cathode electrodes.

We analyzed two different scenarios for tissue filling up defects. In the *acute* defect state, CSF ($\sigma = 1.65$ S/m) was used to fill the hole in the skull (Wagner et al., 2007); CSF has been shown in imaging and

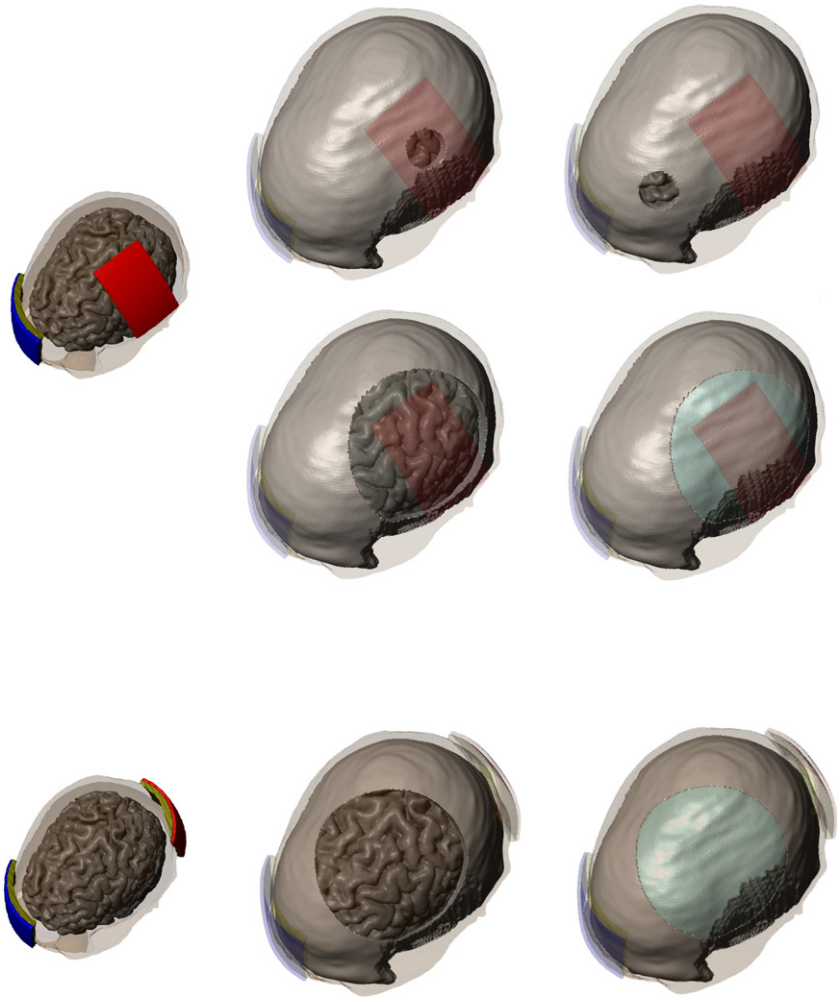

Fig. 1. Healthy and skull injury (defect/plate) simulation montages used to evaluate the effects on cortical current flow in Part 1. Two electrode configurations were evaluated (anode: red, cathode: blue and sponge: olive green). We evaluated the impact of acute or chronic defects (empty skull holes) and skull plates (metallic holes). For the motor cortex anode tDCS, the effect of a small defect under or between the electrodes was evaluated (top row). In addition for motor cortex anode configuration, the effect of large defect or plate under the electrodes was tested (middle row). For occipital cortex anode tDCS, the effect of large defect or plate between the electrodes was tested (bottom row).

histopathology studies to replace damaged tissue in the post acute stage for stroke subjects (Jacobs et al., 2001; Soltanian-Zadeh et al., 2003). In the *chronic* defect state, the hole was replaced by a scar tissue having a combined electrical conductivity of subcutaneous tissue, blood, and meninges compartments ($\sigma = 0.34$ S/m); scar tissue composition will vary across injuries (and indeed over time) such that 0.34 S/m represents an intermediate degree of healing.

Part 1: skull plates — titanium and acrylic

In most of the cases where there is a large skull defect and where the original skull cannot be used to cover the defect, a skull plate is usually indicated for cosmetic purposes and to also protect against external trauma (Sekhar and Fessler, 2006). Therefore another objective in our study was to determine how the presence of skull plates would interfere with the tDCS induced cortical currents. We modeled two material types of skull plates: one made by titanium (one of the most common plates used) with a conductivity of 7.40×10^5 S/m, and acrylic (less common, but a less expensive solution) having a conductivity of 0.20×10^{-12} S/m. We evaluated skull plate only for large skull injuries (10 cm diameter) as usually small skull injuries are not covered with plates. As with acute and chronic skull defects, the skull plates were modeled by replacing a cylindrical hole in the skull by a material; in this case with either titanium or acrylic (Fig. 1).

Part 1: electrode montages

The specific electrode montages implemented for Part 1 are listed in Table 1. For each montage (1–6), the induced cortical currents were analyzed and compared with the analogous healthy head model (Fig. 1).

Part 2: skull defect size

To consider the role of incremental changes in skull defect size, the M1-supraorbital electrode configuration was modeled with different sized skull defects (0.5 cm, 1.5 cm, 3.5 cm, 4.5 cm, 6 cm, and 8 cm diameter). For Part 2 we considered only an *acute* defect state (defect filled with CSF) that was directly underneath the stimulation electrode pads. Note that we did not model skull defects *between* electrode pads, as induced cortical peak electric field values do not differ significantly from the healthy case. For the M1-supraorbital configuration, we considered both a 7×5 cm and a 3.5×3.5 cm *anode* pad — the cathode remained 7×5 cm in all cases. Note that for Part 2, montage designations were not used.

Table 1
Summary of evaluated model montages and simulation results for Part 1. The first column reports the electrode configuration and the second column lists the various montages modeled. The third and the fourth columns specify the type and the location of the defect respectively. For each of these montages, the skull deficit was modeled by replacing the damaged tissue. The deficit was replaced by CSF in the 'acute' phase and by scar tissue in the 'chronic' phase. Column 5 lists either the phase of the deficit or the type of material used for the deficit as applicable. The peak induced electric field magnitude (in V/m) for each of the montages is listed in column 6. Columns 7–9 report the area (in mm^2) of the cortex where the induced EF magnitude was greater than 90%, 80% and 50% of the observed peak EF magnitude respectively.

Electrode configuration	Montage	Skull defect/plate	Location of defect	Phase/plate material	Peak (V/m)	$Area_{90}$	$Area_{80}$	$Area_{50}$
C3-supraorbital	Healthy (*motor cortex tDCS*)	None	–	–	0.67	261.60	720.28	9390.44
	1A	Small hole	Under pad	Acute	2.50	2.75	8.51	220.66
	1B	Small hole	Under pad	Chronic	1.67	7.80	24.74	710.32
	2A	Small hole	Between pads	Acute	0.67	255.62	672.69	7600.87
	2B	Small hole	Between pads	Chronic	0.67	263.22	693.00	7949.73
	3A	Large hole	Under pad	Acute	0.79	190.90	570.56	7208.39
	3B	Large hole	Under pad	Chronic	0.79	239.65	712.46	9287.59
	4A	Large plate	Under pad	Titanium	0.90	88.70	316.46	4324.06
	4B	Large plate	Under pad	Acrylic	0.62	254.09	691.22	7654.99
O1-supraorbital	Healthy (*visual cortex tDCS*)	None	–	–	0.77	186.75	585.39	8519.38
	5A	Large hole	Between pads	Acute	0.72	197.79	583.87	8000.84
	5B	Large hole	Between pads	Chronic	0.73	235.95	723.74	9907.25
	6A	Large plate	Between pads	Titanium	0.91	17.26	96.03	2857.60
	6B	Large plate	Between pads	Acrylic	0.77	184.33	585.08	8612.48

Field solver

A quasi-stationary condition was assumed for the volume conduction in our model. The electric field in a volume conductor is represented as $\nabla\cdot(\sigma\nabla V)=0$ (V: scalar electric potential; ∇: gradient vector; and σ: conductivity). The resulting Laplace equation assuming uniform local conductivity was solved to determine the induced cortical electric field distributions. The boundary conditions used were as follows : (1) inward current flow $=J_n$ (normal current density) applied to the exposed surface of the anode electrode, (2) ground applied to the exposed surface of the cathode electrode, and (3) all other external surfaces treated as insulated. Current densities corresponding to 1 mA total current were applied for each montage. We used COMSOL Multiphysics 3.5 (Comsol Inc., MA), a commercially available finite element (FE) package to implement the model. The linear system iterative solver of conjugate gradients was used with a relative tolerance of 1×10^{-6}.

Surface magnitude plots were generated by plotting the magnitude of electric field (EF) on the surface of brain tissue. Because the conductivity of brain is uniform, these same plots also represent induced current density profiles ($J=\sigma\cdot E$). Additionally, the surface area (in mm^2) of the cortex, where electric field magnitude was greater than 90%, 80% and 50% of the *peak* electric field magnitude was calculated for each montage. These percent *area* measures allow a comparison of the relative focality of induced cortical current flow across different montages (irrespective of peak electric field) — however, it is important to qualify the concept of "focality" when using large sponge electrodes in the context of dispersed clustering of current hot spots throughout the brain (Datta et al., 2009a). The presence of eye balls and fatty tissue owing to their high conductivity provide preferential current pathways that may lead to regions of increased EF magnitude at the bottom of the cortex. In this study, these regions were excluded from the analysis and the peak values reported are from the top surface of the cortex.

Results

We modeled the current distribution in the head during tDCS using two conventional electrode configurations with a range of idealized skull defects or skull plates. We considered the EF magnitude distribution along the cortical surface under the general assumption that both neuromodulation and risk of pathology increase monotonically with EF magnitude (see Discussion). For Part 1, the effects of skull injuries on the location and magnitude of peak cortical EF, as well as the EF distribution was analyzed (Table 1). For Part 2, the variation of induced cortical electric fields with skull defect size was determined. Evidently it is not possible to explicitly consider all permutations of electrode configuration and defect/plate montages, nor can our results using a specific head anatomy be arbitrarily and quantitatively generalized (see Discussion); rather the goal of this analysis is to identify what factors modulate current flow through the brain and develop a general framework for identifying how these factors interact. Ultimately, such knowledge would provide a basis for designing tDCS electrotherapies in patients with TBI or surgical skull defects.

Healthy skull montage

In order to explore the effects of skull injuries on cortical currents, it is necessary to compare with a healthy head model in which the skull is intact. We therefore adapted a high-resolution (sulci/gyri precise) healthy model developed previously. Consistent with our previous predictions, using either the M1 or occipital anode "large sponge" electrode configurations resulted in diffuse modulation over the entire cortical surface with numerous discrete clusters of local EF maxima (in contrast with the controlled focality of high-definition tDCS; (Datta et al., 2009a,b)). The observance of these localized clusters/hot spots reinforces the importance of incorporating detailed cortical geometry in any tDCS modeling study.

A total current of 1 mA injected through the electrodes resulted in a 0.67 V/m and 0.77 V/m peak cortical EF magnitudes for the M1 and occipital anode configurations, respectively. These values are compatible to predictions from previous tDCS FEM models (Miranda et al., 2006; Wagner et al., 2007).

Using large sponge configurations, any consideration of focality and targeting must be qualified. M1 anode electrode configuration resulted in more than 9000 mm^2 of cortex being at or above 50% of the peak cortical EF; moreover the peak EF was between and not under the sponges (Fig. 2, top row). Using the Occipital anode electrode configuration, more than 8500 mm^2 of cortex was at or above 50% of peak cortical EF, with the peak clustered under the lateral edge of one pad (Fig. 4, top row).

Part 1: small skull defect (Fig. 2 — montages 1 and 2)

The presence of a small defect (diameter = 2.5 cm) in the skull directly underneath the pad (Montage 1) creates a preferential conduit for radial currents into the cortex; thus, altering the spatial profile of current flow as compared to the healthy model (Fig. 2). Specifically, this montage results in a 'focal' region of modulation with increased induced EF/current density magnitude that has roughly the dimensions of the overlying skull hole.

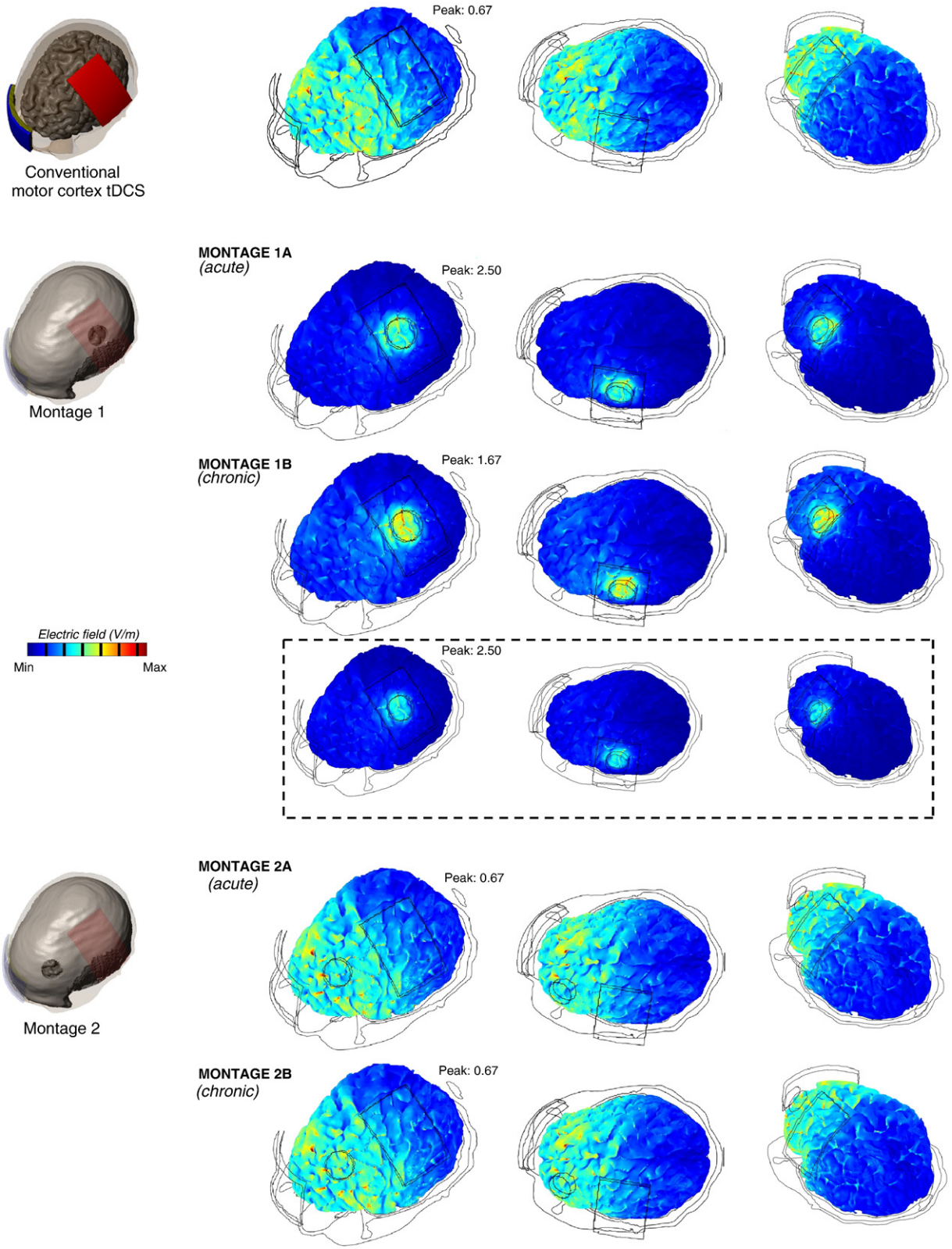

Fig. 2. Brain modulation of *small skull defects* during tDCS. Each of the rows show the surface magnitude plots of induced electric field magnitude (with different views). The second column shows the top view, while the third column shows the side view revealing modulation in the posterior lobes. The first row models the C3-supraorbital configuration (healthy model) thereby enabling comparison with the head models having skull defects. The second and third rows show the modeling results for Montage 1 with acute and chronic states respectively (see Methods). Likewise, the fifth and the sixth rows plot the simulation results for Montage 2. The fourth row shows the modeling results for Montage 1B re-scaled to the *peak* value of EF induced in Montage 1A.

The observed peak EF magnitude in the cortex is strongly influenced by the conductivity value of the material filling the skull defect. The acute phase (defect filled with CSF) and chronic phase (defect filled with scar tissue) resulted in peak EF magnitude of 2.50 and 1.67 V/m respectively. Thus in Montage 1, for the acute phase, the induced EF magnitude increases to ~3.7 times than that for a healthy

head model (Part 2 below addresses the specific role of defect size in more detail).

In all cortical field plots, the false-color map is scaled to the respective peak cortical EF. Only for the case of Montage 1B, where we also re-scaled the color map to correspond to the peak value observed for Montage 1A (Fig. 2, box); it becomes apparent that Montage 1B results in reduced cortical activation under the defect compared to Montage 1A. This was done to emphasize the importance of *not* directly comparing false-color plots across montages without correcting for the different scales used.

In contrast, when the small skull defect location is *between* the two electrode pads (Montage 2), there was not a marked change in the spatial profile of current flow through the cortex (Fig. 2). In fact, similar peak EF magnitude as that of the healthy model is observed in both the acute and chronic states. This finding highlights that the *specific location* of the defect critically influences the flow of cortical currents.

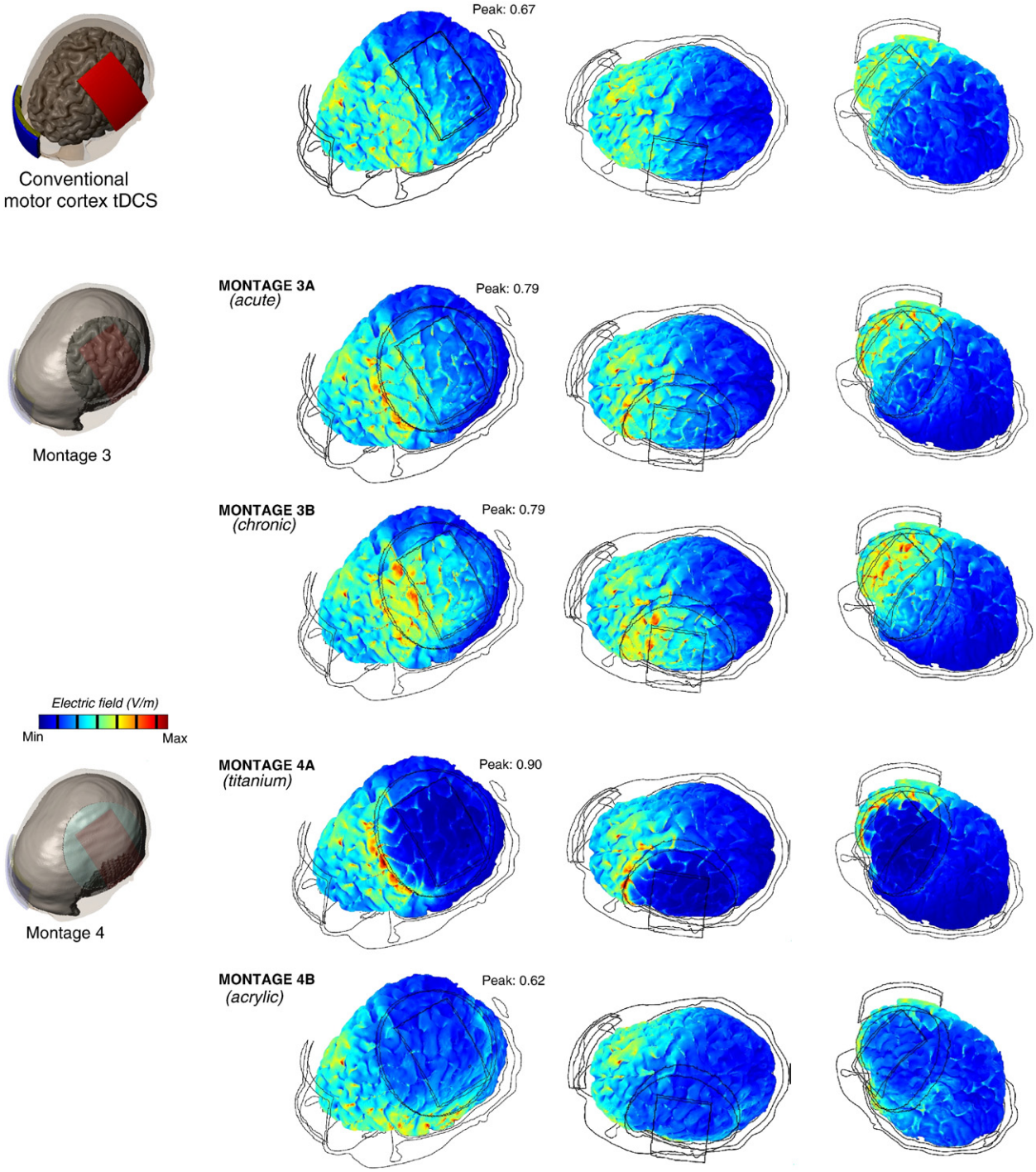

Fig. 3. Brain modulation of *large skull defects* and *skull plates* during motor cortex tDCS. Each of the rows shows the surface magnitude plots of induced electric field magnitude (with different views). The second column shows the top view, while the third column shows the side view revealing modulation in the posterior lobes. The first row models the C3-supraorbital configuration (healthy model). The second and third rows show the modeling results for Montage 3 with *acute* and *chronic* states respectively (see Methods). The fourth and the fifth rows plot the simulation results for Montage 4 with *titanium* and *acrylic* skull plates respectively.

Part 1: large skull defects (Figs. 3 and 4 — montages 3 and 5)

The presence of a large defect (diameter = 10 cm) in the skull directly underneath the pad (Montage 3) alters the spatial profile as compared with the healthy head model. The peak induced EF magnitude was 0.79 V/m in both the acute and chronic phases (Fig. 3). However, in spite of similar peak EF magnitudes, the region of cortical modulation is influenced by the conductivity value of the defect. Peak EF magnitude was observed in the cortex directly underneath the hole in the chronic case while for the acute phase, the peak EF magnitude was observed in cortex corresponding to the edge of the hole.

For the case where the defect was between the two electrodes (Montage 5), the current is initially induced in the posterior lobes and then is shunted across the hole (Fig. 4). The amount of shunt depends on the electrical conductivity of the hole. The peak induced EF

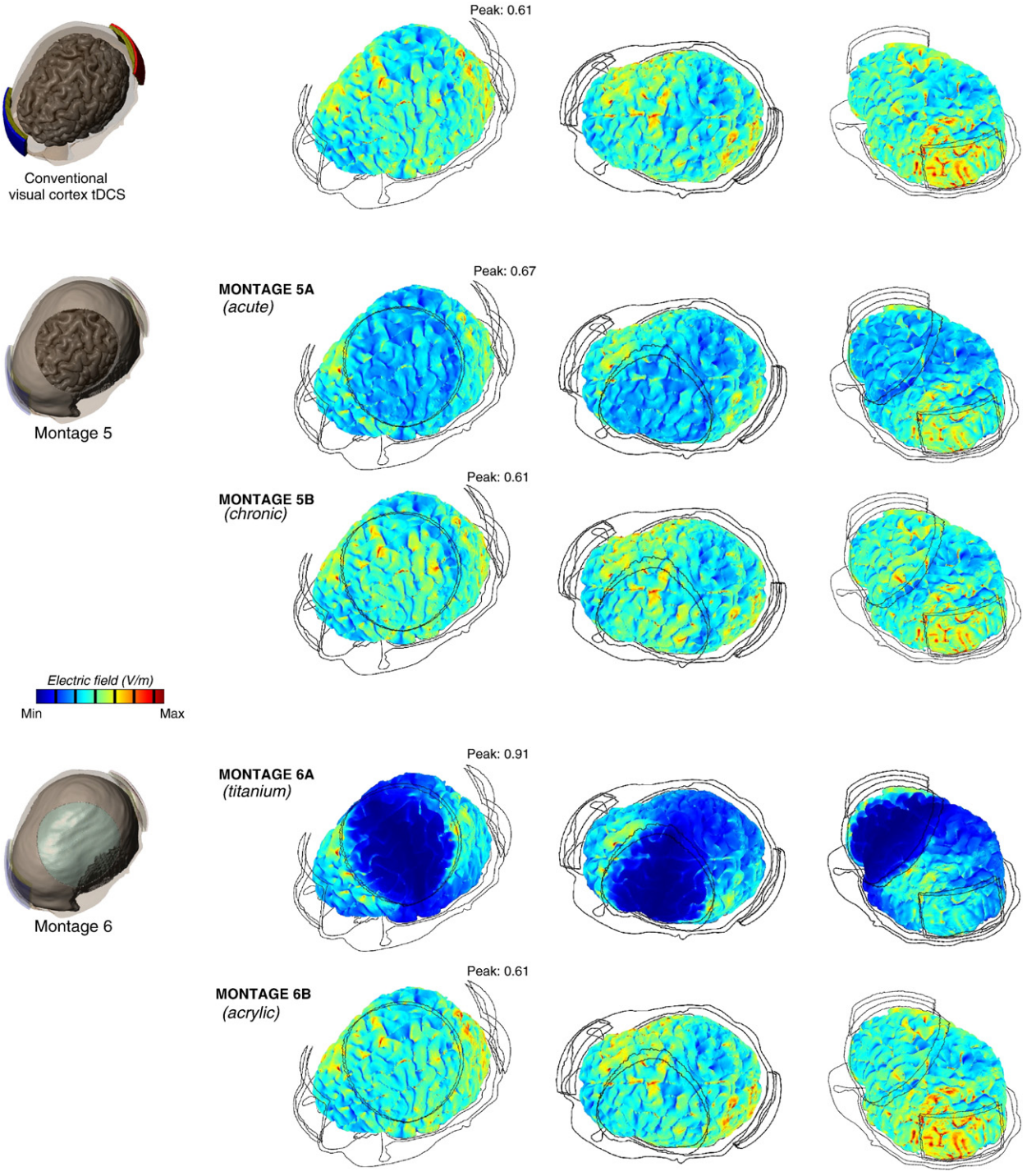

Fig. 4. Brain modulation of *large skull defects* and *skull plates* during visual cortex tDCS. Each of the rows show the surface magnitude plots of induced electric field magnitude (with different views). The second column shows the top view, while the third column shows the side view revealing modulation in the posterior lobes. The first row models the O1-supraorbital configuration (healthy model). The second and third rows show the modeling results for Montage 5 with *acute* and *chronic* states respectively (see Methods). The fourth and the fifth rows plot the simulation results for Montage 6 with *titanium* and *acrylic* skull plates respectively.

magnitude in the acute and chronic cases was similar to that of the healthy head model.

The primary effect of large skull defects (with increasing conductivity relative to the skull) can be broadly described as *reducing* current flow crossing into the underlying cortex by shunting (transverse to the cortical surface) while concentrating current in the cortex underlining the skull defect edge. The aforementioned effect is however observed to be more pronounced with proximity of the defect to the stimulation pad.

Part 1: skull plates (Figs. 3 and 4 — montages 4 and 6)

Due to its very high conductivity, the presence of a titanium plate accentuates the shunting effect observed with large skull defects. The region of modulation is generally restricted to the portion of the cortex corresponding to the edge of the defect and negligible modulation is observed directly underneath the plate. In addition, the rises in the peak induced EF magnitude (for both under and between the pads) in comparison to the healthy head model are more than that observed with large skull defects.

The effects of acrylic plates on the underlying cortical flow are much less pronounced. There is a negligible difference in both the overall spatial profile and the peak induced EF magnitude in comparison with the healthy model (Montage 6B). For the case of acrylic plate under the pads (Montage 4B), there is a nominal decrease in the peak EF magnitude in comparison to the healthy model.

Part 2: skull defect size

The values of induced cortical EF magnitudes are maximal when the skull defect size approximates the dimension of the stimulation pad and then decreases when skull defect size is either very small or large (Fig. 5). A similar trend was observed with both the 7×5 cm and 3.5×3.5 cm stimulation pads. However, for the 7×5 cm case, the observed peak induced current density in the brain, for a skull defect range of ~3.5 cm, was found to *exceed* the average injected scalp electrode current density (total injected current/electrode area).

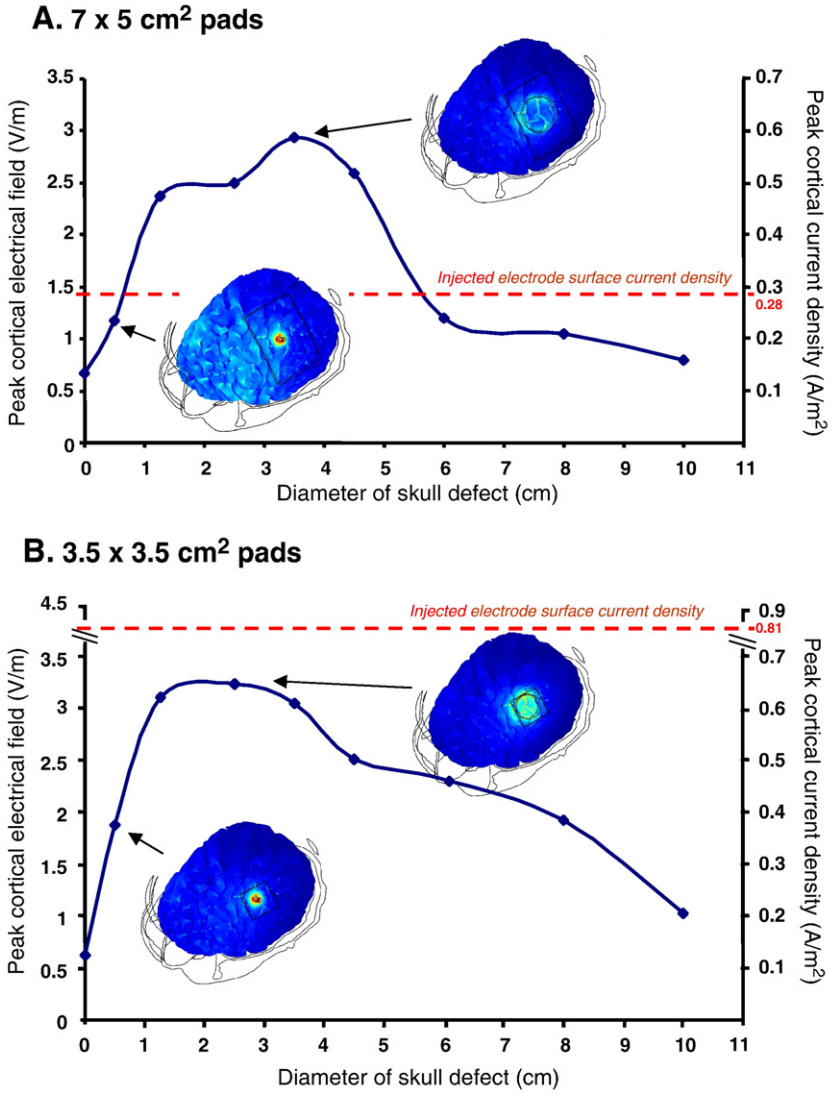

Fig. 5. Role of skull defect size in shaping brain modulation during tDCS. In Part 2, acute defects were fixed under the motor cortex anode. Two anode electrodes sizes were evaluated: A) 7×5 cm and B) 3.5×3.5 cm with a range of acute skull defect diameters and for the healthy case (e.g. 0 diameters skull defect) case. Peak cortical electric field and peak cortical current density (which are linearly related) are graphed with selected cases expanded as cortical surface plots (scaled to the respective peak cortical electric field). For both electrodes, 1 mA of current was applied resulting in average electrode current densities of (0.28 and 0.81 A/m^2 respectively corresponding to the dashed red lines).

Under both the 7 × 5 cm and 3.5 × 3.5 cm pads, the presence of very small defects (0.5 cm diameter) doesn't increase the peak induced electric field significantly relative to the healthy head model. As the skull defect size becomes smaller, less current shunts through the defect into the underlying cortex eventually approximating the spatial profile observed in the healthy (no defect) case (see Fig. 5).

Discussion

Our results confirm the notion that skull defects and skull plates can change the distribution of the current flow induced in cortical areas by tDCS; however, the details of current modulation depend entirely on the combination of electrode configuration and nature of the defect/plate. In majority of cases, with the notable exemption of a moderate defect directly under an electrode, the presence of defects does not result in a marked increase in peak cortical electric field magnitude, though the distribution of electric field and the location of the peaks are shifted toward defect edges.

Altered current flow around skull defects and plates

We propose a relatively parsimonious framework to explain the range of observation in this study. Under healthy conditions, we previously showed that current is first distributed laterally across the skin and then crosses the skull in a largely radial manner; the current is *not* distributed through the skull (as previously contended). After passing the skull the current travels through the higher-conductivity CSF network, where it can be both distributed and concentrated; and before crossing into the brain, current patterns may be dominated by CSF which offers a pathway with much lower resistance. For the case of a small to moderate size defect with increased conductivity relative to skull, the defect acts as a preferential pathway for current to cross radially (compared to the surrounding skull) and into the brain leading to a "funnel" type phenomena (Datta et al., 2009a). The maximal concentration of cortical current is a function of several factors including defect size relative to electrode size. Importantly, the conditions at the surface (skin) still determine if there is a driving force for current to enter or exit at the location of the defect, so for the case of a small defect in the middle of two electrodes there is not enough driving force and no significant radial current flow at that location under normal conditions — as such, the defect does not change the overall current flow pattern.

For the case of a large defect/plate, with conductivity significantly higher than skull, the current may now travel tangentially along the defect/plate, moving between the electrodes. This new defect/plate pathway may be comparable in conductivity to that of the underlying tissue (e.g. chronic defect) or the new pathway may be more conductive than the underlying tissue (e.g. acute defect and especially the titanium plate). The fraction of current "diverted" through the defect increases with both defect conductivity and defect proximity to an electrode. In the extreme conductivity case of titanium, the current preferentially travels tangentially along the plate, avoiding underlying tissue, until reaching the defect/plate edge at which point the current enters the tissue radially rather than continue in the highly-resistive skull.

Similar considerations can explain the range of EF distribution observed under conditions of defects and plates (Figs. 2, 3, 4, and 5), though we emphasize that the ultimate pathway of current flow through the brain is rather complex and determined by the combination of all tissue geometries and properties (Datta et al., 2009a). None-the-less, our results indicate that a gross consideration of the idealized defect/plate properties relative to the electrode configuration can be used to intuitively predict the qualitative alterations of current flow.

Clinical and safety considerations

The success of tDCS treatments for depression, stroke and chronic pain warrants evaluation of safety of this therapy in patients with skull defects/injuries. This is an important issue since a relatively large proportion of patients might have skull defects and skull plates such as patients with stroke, who underwent decompression craniectomy, or patients with refractory epilepsy who undergo epilepsy surgery and finally patients with traumatic brain injury that commonly have skull fractures or need to undergo craniectomy. To date, there are no studies assessing the effects of tDCS in these patients. Evidently, safety studies in patients with skull plates for other brain stimulation modalities (e.g. TMS; Rotenberg et al., 2007; Rotenberg and Pascual-Leone, 2009) cannot be substituted.

The central clinical relevance of this initial study is that skull injuries significantly change the distribution of the current being induced in cortical areas. As highlighted in this work, our models predict that current may become concentrated over the edges of large skull defects/plates. Interestingly, similar edge effect is seen in another study where tDCS fields were computed for stroke lesions filled with CSF (Wagner et al., 2007). Importantly, for the range of *large* skull defect/plate configurations tested in the present study, no significant change in peak cortical EF (i.e. 1.5 times than that for a healthy head) resulted, despite changes in distribution. This result suggests that although theoretically safe, stimulation with large skull defects might not induce the aimed clinical effects if different areas are stimulated. In fact, although tDCS induces relatively widespread (un-focal) effects, position of electrodes and induced current is critical (Fregni et al., 2005a). In this case, the next important question is whether, it is possible then to vary electrode's position to induce currents in areas that were affected by the skull defect.

Another important finding of this study is that the current peak does not change significantly, except for moderately sized defects when the stimulation electrode is placed directly over the defect (Fig. 5). This increase in current peak magnitude in comparison with the control (healthy) case may therefore pose potential safety concerns. Investigation in animals has suggested that the brain currents induced in healthy adults during conventional tDCS are two orders of magnitudes below intensities causing brain lesions (for the cathodal case; Liebetanz et al., 2009) or electrographic seizures (for the anodal case; Bikson et al, 2004). If the degree of concentration due to the skull defect can be predicted, a simple mitigating measure would be to decrease the total injected current. Conversely, if the desired targeted brain region was under the skull defect, positioning an electrode over a small defect could be used to focus the current into the targeted region. Generally as defect size decreases, cortical modulation becomes concentrated under the defect and peak induced cortical electric fields increases. However, further decreases in defect size can *decrease* peak cortical electric field even as the relative profile of brain modulation continues to become more targeted. Still further decreases in defect size result in a shift toward the healthy (no defect) case.

There has been debate about the relative merits of "normalizing" tDCS dose to average current density at the electrode surface (Miranda et al., 2009; Nitsche et al., 2007). Our results with skull defects support a tDCS dose system based on a consideration of the entire detailed electrode configuration (Bikson et al., 2008); moreover, *individual* differences and especially skull defects/plates will modulate how given electrode montages affect brain function. In this context it is important to consider that skull deficits will significantly vary across patients especially if associated with skull loss due to TBI and skull fracture; in each case the factors of defect size and position in relation to the electrodes can be generally considered according to the results of our study.

The modeling predictions presented in this paper present an initial evaluation and must be interpreted cautiously with regard to clinical

application, especially pending experimental validation. Nevertheless the parsimonious guidelines suggested by our simulation results are a step toward the design of safe and efficacious tDCS therapies/protocols for patients with skull defects.

Uses and limitations of the present FEM study

Because of the critical dependence on material properties (tissue electrical conductivity) and brain skin/brain anatomy, reduced phantoms are of limited use in predicting *cortical* current flow (Rush and Driscoll, 1968; Leahy et al., 1998). Similarly, though animal studies are pivotal in addressing biophysical mechanisms of action, they are ill-suited for the design of tDCS electrode montages. "Forward" models of induced current flow are a standard tool in electrotherapy design (Butson et al., 2007), and are theoretically constrained by simple physical assumptions (e.g. Ohms law). The accuracy of model predictions is however limited by accuracy and precisions of model anatomy and parameterization. For example, our observation of stimulation clustering reinforces the importance of models incorporating sulci/gyri resolution (Datta et al, 2009a). Conversely, we expect analogous gross distortions of current flow, following our parsimonious guidelines, may generalize even to spherical models (Miranda et al., 2006; Datta et al., 2008).

Our study has some limitations that need to be entertained in the context of progressing with animal experimentation and eventually clinical trials: 1) we considered only cortical surface electric field magnitude in this study under the assumptions that the cortical surface is of primary interest in tDCS efficacy/safety and that both the degree of neuronal modulation and the risk of injury increase monotonically with electric field magnitude. This approach does not address the nature or specific thresholds for any physiological or pathological effects, the importance of neuronal geometry relative to applied fields (Radman et al., 2009; modulation maps in Datta et al., 2008) or the complex dynamic response of the brain to stimulation (Bikson et al., 2004); 2) the role of baseline individual differences (e.g. gross anatomy) was not considered; 3) moreover, the nature of defects is expected to vary significantly across cases and may be paramount in determining the details of current flow; 4) the defects considered here were highly idealized, since one would expect complex geometries and in-homogeneous tissue properties (including tissue encapsulation) in realistic injuries; 5) and finally an important issue is that skull defects and skull plates are usually seen in patients with cortical damage and because we modeled only one healthy adult male brain, it is conceivable that cortical lesions would cause additional disturbances in the current being induced by tDCS. Such changes could affect current flow within the damaged region and through adjacent regions in a complex manner. For all the reasons indicated, *individualized* models for patients with brain and skull lesions are the best approach to predict with some accuracy maximal currents and current distributions. Despite these significant limitations in extrapolating *quantitative* generalization from the present study, the qualitative characterization of the general combination of factors which lead to altered current flow in cases of skull defects/plates provides a basis to understand how skull defects would affect current intensity and distribution and therefore can be helpful to set out inclusion and exclusion criteria of patients with skull defects. The next step is to perform experimental/functional assessments (such as testing cortical excitability changes) to confirm these predictions.

Acknowledgments

We acknowledge Viet Bui Xuan of Simpleware Ltd.; and Varun Bansal and Davide Reato of The City College of New York. Felipe Fregni is partially funded by CIMIT (Center for Integration of Medicine and Innovative Technology). Marom Bikson is partially funded by NIH (nos. S06GM008168 NS054783) and the Wallace H. Coulter Foundation.

References

Ardolino, G., Bossi, B., Barbieri, S., Priori, A., 2005. Non-synaptic mechanisms underlie the after-effects of cathodal transcutaneous direct current stimulation of the human brain. J. Physiol. 568, 653–663.

Bikson, M., Inoue, M., Akiyama, H., Deans, J.K., Fox, J.E., Miyakawa, H., et al., 2004. Effects of uniform extracellular DC electric fields on excitability in rat hippocampal slices in vitro. J. Physiol. 557, 175–190.

Bikson, M., Bulow, P., Stiller, J.W., Datta, A., Battaglia, F., Karnup, S.V., et al., 2008. Transcranial direct current stimulation for major depression: a general system for quantifying transcranial electrotherapy dosage. Curr. Treat. Options Neurol. 10, 377–385.

Boggio, P.S., Bermpohl, F., Vergara, A.O., Muniz, A.L., Nahas, F.H., Leme, P.B., et al., 2007. Go-no-go task performance improvement after anodal transcranial DC stimulation of the left dorsolateral prefrontal cortex in major depression. J. Affect. Disord. 101, 91–98.

Boggio, P.S., Liquori, P., Sultani, N., Rezende, L., Fecteau, S., Fregni, F., 2009a. Cumulative priming effects of cortical stimulation on smoking cue-induced craving. Neurosci. Lett. 463, 82–86.

Boggio, P.S., Zaghi, S., Fregni, F., 2009b. Modulation of emotions associated with images of human pain using anodal transcranial direct current stimulation (tDCS). Neuropsychologia 47, 212–217.

Butson, C.R., Noecker, A.M., Maks, C.B., McIntyre, C.C., 2007. StimExplorer: deep brain stimulation parameter selection software system. Acta Neurochir. Suppl. 97, 569–574.

Chew, E., Straudi, S., Fregni, F., Zafonte, R.D., Bonato, P., 2009. Transcranial direct current stimulation enhances the effect of upper limb functional task training in neurorehabilitation. Abstract presented at 5th World Congress of ISPRM.

Datta, A., Elwassif, M., Battaglia, F., Bikson, M., 2008. Transcranial current stimulation focality using disc and ring electrode configurations: FEM analysis. J. Neural Eng. 5, 163–174.

Datta, A., Bansal, V., Diaz, J., Patel, J., Reato, D., Bikson, M., 2009a. Gyri-precise head model of transcranial direct current stimulation: improved spatial focality using a ring electrode versus conventional rectangular pad. Brain Stimul. 2, 201–207.

Datta, A., Elwassif, M., Bikson, M., 2009b. Bio-heat transfer model of transcranial DC stimulation: comparison of conventional pad versus ring electrode. Conf. Proc. IEEE Eng. Med. Biol. Soc. 670–673.

Fregni, F., Boggio, P.S., Nitsche, M.A., Bermpohl, F., Antal, A., Feredoes, E., et al., 2005a. Anodal transcranial direct current stimulation of prefrontal cortex enhances working memory. Exp. Brain Res. 166, 23–30.

Fregni, F., Simon, D.K., Wu, A., Pascual-Leone, A., 2005b. Non-invasive brain stimulation for Parkinson's disease: a systematic review and meta-analysis of the literature. J. Neurol. Neurosurg. Psychiatry 76, 1614–1623.

Fregni, F., Boggio, P.S., Lima, M.C., Ferreira, M.J., Wagner, T., Rigonatti, S.P., et al., 2006a. A sham-controlled, phase II trial of transcranial direct current stimulation for the treatment of central pain in traumatic spinal cord injury. Pain 122, 197–209.

Fregni, F., Thome-Souza, S., Nitsche, M.A., Freedman, S.D., Valente, K.D., Pascual-Leone, A., 2006b. A controlled clinical trial of cathodal DC polarization in patients with refractory epilepsy. Epliepsia 47, 335–342.

Fregni, F., Freedman, S.D., Pascual-Leone, A., 2007. Recent advances in the treatment of chronic pain with non-invasive brain stimulation techniques. Lancet Neurol. 6, 188–191.

Hummel, F., Celnik, P., Giraux, P., Floel, A., Wu, W.H., Gerloff, C., et al., 2005. Effects of non-invasive cortical stimulation on skilled motor function in chronic stroke. Brain 128, 490–499.

Iyer, M.B., Mattu, U., Grafman, J., Lomarev, M., Sato, S., Wassermann, E.M., 2005. Safety and cognitive effect of frontal DC brain polarization in healthy individuals. Neurology 64, 872–875.

Jacobs, M.A., Zhang, Z.G., Knight, R.A., Soltanian-Zadeh, H., Goussev, A.V., Peck, D.J., et al., 2001. A model for multiparametric MRI tissue characterization in experimental cerebral ischemia with histological validation in rat: part 1. Stroke 32, 943–949.

Leahy, R.M., Mosher, J.C., Spencer, M.E., Huang, M.X., Lewine, J.D., 1998. A study of dipole localization accuracy for MEG and EEG using a human skull phantom. Electroencephalog. Clin. Neurophysiol. 107, 159–173.

Liebetanz, D., Nitsche, M.A., Tergau, F., Paulus, W., 2002. Pharmacological approach to the mechanisms of transcranial DC-stimulation-induced after-effects of human motor cortex excitability. Brain 125, 2238–2247.

Liebetanz, D., Klinker, F., Hering, D., Koch, R., Nitsche, M.A., Potschka, H., et al., 2006. Anticonvulsant effects of transcranial direct-current stimulation (tDCS) in the rat cortical ramp model of focal epilepsy. Epliepsia 47, 1216–1224.

Liebetanz, D., Koch, R., Mayenfels, S., Konig, F., Paulus, W., Nitsche, M.A., 2009. Safety limits of cathodal transcranial direct current stimulation in rats. Clin. Neurophysiol. 120, 1161–1167.

Miranda, P.C., Lomarev, M., Hallett, M., 2006. Modeling the current distribution during transcranial direct current stimulation. Clin. Neurophysiol. 117, 1623–1629.

Miranda, P.C., Faria, P., Hallett, M., 2009. What does the ratio of injected current to electrode area tell us about current density in the brain during tDCS? Clin. Neurophysiol. 120, 1183–1187.

Nitsche, M.A., Fricke, K., Henschke, U., Schlitterlau, A., Liebetanz, D., Lang, N., et al., 2003. Pharmacological modulation of cortical excitability shifts induced by transcranial direct current stimulation in humans. J. Physiol. 553, 293–301.

Nitsche, M.A., Doemkes, S., Karakose, T., Antal, A., Liebetanz, D., Lang, N., et al., 2007. Shaping the effects of transcranial direct current stimulation of the human motor cortex. J. Neurophsyiol. 97, 3109–3117.

Radman, T., Ramos, R.L., Brumberg, J.C., Bikson, M., 2009. Role of cortical cell type and morphology in sub- and suprathreshold uniform electric field stimulation. Brain Stimul. 2, 215–228.

Rish, L., Dillon, J.D., Meirowsky, A.M., Caveness, W.F., Mohr, J.P., Kistler, J.P., et al., 1979. Cranioplasty: a review of 1030 cases of penetrating head injury. Neurosurgery 4, 381–385.

Rotenberg, A., Pascual-Leone, A., 2009. Safety of 1 Hz repetitive transcranial magnetic stimulation (rTMS) in patients with titanium skull plates. Clin. Neurophysiol. 120, 1417.

Rotenberg, A., Harrington, M.G., Birnbaum, D.S., Madsen, J.R., Glass, I.E., Jensen, F.E., et al., 2007. Minimal heating of titanium skull plates during 1 Hz repetitive transcranial magnetic stimulation. Clin. Neurophysiol. 118, 2536–2538.

Rush, S., Driscoll, D.A., 1968. Current distribution in the brain from surface electrodes. Anesth. Analg. 47, 717–723.

Sekhar, L., Fessler, R., 2006. Atlas of Neurosurgical Techniques. Brain Thieme, New York.

Soltanian-Zadeh, H., Pasnoor, M., Hammoud, R., Jacobs, M.A., Patel, S.C., Mitsias, P.D., et al., 2003. MRI tissue characterization of experimental cerebral ischemia in rat. J. Magn. Reson. Imaging 17, 398–409.

Wagner, T., Fregni, F., Fecteau, S., Grodzinsky, A., Zahn, M., Pascual-Leone, A., 2007. Transcranial direct current stimulation: a computer-based human model study. Neuroimage 35, 1113–1124.